SEMARAK ILMU PUBLISHING

CFD Letters

Journal homepage:
https://semarakilmu.com.my/journals/index.php/CFD_Letters/index
ISSN: 2180-1363

Sensitivity of TBL Wall-Pressure over the Flat Plate on Numerical Turbulence Model Parameter Variations

Biplab Ranjan Adhikary[1,*], Ananya Majumdar[1], Atanu Sahu[2], Partha Bhattacharya[1]

[1] Department of Civil Engineering, Jadavpur University, Kolkata, West Bengal, India
[2] Department of Civil Engineering, National Institute of Technology, Silchar, Assam, India

ARTICLE INFO

Article history:
Received 12 December 2022
Received in revised form 13 January 2023
Accepted 11 February 2023
Available online 1 July 2023

Keywords:
TBL; sensitivity; spectrum model; RANS; CFD

ABSTRACT

A two-fold sensitivity of the zero-pressure gradient (ZPG) turbulent boundary layer (TBL) wall-pressure spectrum to different RANS model parameters is investigated for a flat plate case, which is a close approximation to the aircraft fuselage or wing. The alteration in the mean square pressure fluctuations due choice of semi-empirical pressure model and the choice of computational model parameters like solver, near wall grid clustering, measuring location, and flow velocity are separately studied. The underlying effect of different TBL parameters in the said sensitivity has been studied while numerically replicating wind tunnel experiments and in-flight tests considering different RANS configurations. Initially, the best-predicting pressure spectrum models are selected by comparing them with available in-flight and wind tunnel test data. Subsequently, the accuracy of all the individual model parameters in predicting mean TBL flow quantities like wall shear stress, boundary layer thickness, displacement thickness, momentum thickness, etc., and eventually mean square pressure (MSP) is estimated. The sensitivity of the mean square pressure fluctuations value to the TBL flow quantities and the near-wall grid clustering is observed to be significant. In general, $k-\omega$ family of models is found to be best in terms of numerical convergence and closeness when compared to the experimental MSP values. $k-\epsilon$ family of models is suggested to be avoided while estimating MSP in flat plate TBL case.

1. Introduction

Turbulent boundary layer (TBL) wall-pressure fluctuation is one of the key parameters for vibro-acoustic response prediction of TBL-excited flat flexible panels, an approximation to the aircraft fuselage or wing. Flight tests are the final phase of testing the prototype to ensure safety and satisfactory performance. It is likely to be a labour-intensive, chronophagous and exorbitant affair. To mitigate this, modern techniques of wind tunnel experiments and computational fluid dynamics (CFD) are performed. Accurate and faster prediction of wall-pressure fluctuation leads to the better understanding of the structural vibration and hence dictates alteration in the early design stage.

* *Corresponding author.*
E-mail address: biplab.iitkgp@yahoo.com (Biplab Ranjan Adhikary)

https://doi.org/10.37934/cfdl.15.7.148174

Various wind tunnel experiments have been conducted by many researchers for studying the wall pressure fluctuations in turbulent boundary layer (TBL). Schewe [1] investigated the statistical properties of the characteristic wall pressure structures by signal averaging, its connection with the phenomena occurring in the buffer layer and visual analysis in the time domain. Experiments conducted by McGrath *et al.,* [2] lead to obtaining rational and consistent surface pressure fluctuation results for zero and favourable pressure gradient flows. The recognition of the turbulent source regions within the boundary layer that contribute to the frequency spectra of low-, mid-, and high-frequency ranges of the wall pressure field and frequency cross-spectra of the wall pressure fluctuations beneath a fully developed turbulent boundary layer was done by Farabee *et al.,* [3]. Experiments of Gravante *et al.,* [4], indicated that the wall region of the boundary layer is the governing source of the high-frequency pressure fluctuations. Experiments to measure surface pressure fluctuations beneath low Reynolds number, two-dimensional turbulent boundary layers and high Reynolds-number three-dimensional boundary layers were performed by Goody and Simpson [5]. Rackl and Weston [6] best predicted the low to medium frequency. Rocha and Palumbo [7] investigated the sensitivity of fuselage sidewall sound radiation corresponding to changes in TBL parameters. Wall pressure fluctuations measurement and direct measurements of wavevector-frequency spectra have been performed by Salze *et al.,* [8]. A statistical post-processing technique was developed by Blitterswyk and Corey [9] for extracting coherent motions using intermittency of energy in the wavelet coefficients. Shahmohamadi and Rashidi [10] conducted experiments on a flat plate in a wind tunnel and suggested two new correlations for the friction coefficient and boundary layer thickness as functions of Reynolds number. All these experimental studies essentially performed in order to not only estimate the TBL wall-pressure fluctuations but to develop empirical and semi-empirical pressure-spectrum models, few of which are discussed further.

Data from the wind tunnel experiments or CFD are fetched into semi-empirical model to estimate zero pressure gradient (ZPG) turbulent boundary layer (TBL) wall-pressure spectrum models with different TBL parameters. There are several semi-empirical single-point wall-pressure spectrum models available and widely used for practical purposes. However, these models are essentially dependent on the feeding of the experimental data. In one of the latest works, Thomson and Rocha [11] compared different wind tunnel and in-flight test results with available semi-empirical spectrum models for zero pressure gradient cases. They have found Goody [12] and Smol'yakov [13] models to be the best predictor of the wind tunnel test results. Leneveu *et al.,* [14] carried out CFD simulation using OpenFOAM solver, based on the experimental data of Salze *et al.,* [8]. Dominique *et al.,* [15] used an artificial neural network (ANN) that is trained with existing experimental and CFD results and predicts better spectrum formulation, especially for the adverse pressure gradients.

But experiments are expensive and often non-compliant to the variation of in-flow parameters or the orientation of the flat plate. To further ameliorate the process, flow parameters are simulated numerically using computational fluid dynamics (CFD). In this work, the Navier-Stokes equations are closed using the RANS turbulence models. With the increasing computing capacity, CFD simulations have emerged to fill the gap. Although direct numerical simulation (DNS) and large eddy simulation (LES) are proven to be robust and more accurate, considering the computation cost, nowadays RANS techniques are most commonly used for industrial purposes. However, all the RANS models do not provide a similar level of accuracy for predicting TBL parameters. Their accuracy changes from case to case. A change in y^+ values or even a change in the solver, alters the accuracy. Moreover, the universal velocity plot (y^+ vs U^+) cannot be the only determining factor for the prediction of the wall-pressure fluctuations. Furthermore, due to the differences in the route of their development, wall-pressure spectrum models are differently sensitive to the TBL parameters. Therefore, extensive research work required to fill the above-mentioned gap has been presented in this paper, to a)

identify the best spectrum model to predict wind tunnel experiments and in-flight test results, b) quantify the accuracy of different solvers, CFD turbulence closure models and y^+ values in comparison to the experimental results, c) quantify the split in the contribution of approximation in spectrum models and turbulence models toward the accumulated error. The present study will definitely serve as comprehensive documentation for future researchers in the said domain.

2. Mathematical Formulations

The mathematical formulations for the present study are presented in this section. First, the important single-point wall-pressure spectrum models are described. These spectra are estimated using respective experimental mean TBL flow quantities in MATLAB (R2013b) environment. Next, several RANS closure models are described which are subsequently solved using finite volume based CFD solvers, OpenFOAM (v-2012 in Ubuntu 20.04) and ANSYS Fluent (V14.5), with varying model parameters. The estimated flow quantities are then used as input to the semi-empirical models, and the accuracy of the RANS model configurations is studied.

2.1 Semi-Empirical Models

The TBL pressure spectra proposed by various researchers that have been used in this study are Efimtsov Model [28], Rackl and Weston Model [6], Lowson Model [29], Chase-Howe Model [30, 31], Lagnelli Model [32], Goody Model [12], Smol'yakov Model [13] and Smol'yakov and Tkachenko Model [16]. The mathematical description for three of these models is described below, to demonstrate the complex relationship between the pressure spectrum and the TBL parameters. Moreover, these three models work very well, particularly in the case of flow-induced plate vibration studies in a wind tunnel [16] and in-flight tests [6, 28]

2.1.1 Smol'yakov and Tkachenko model [16]

The single-point wall-pressure spectrum Φ_p is calculated as:

$$\Phi_p(\omega) \approx \left(\frac{\tau_w \delta^*}{U_0}\right)\left(\frac{5.1}{1+0.44\left(\frac{\omega\delta^*}{U_0}\right)^{\frac{7}{3}}}\right) \tag{1}$$

$$\tau_w \approx \frac{0.0225\rho U_0^2}{{Re_\delta}^{0.25}} \tag{2}$$

where U_0 is the free-stream flow velocity and δ^* is the boundary layer displacement thickness. In the case of TBL flow with zero pressure gradient wall shear stress τ_w can be estimated as in Eq. (2), where Re_δ is the boundary layer thickness Reynolds number given by $Re_\delta \approx 8U_0\delta^*/\nu$, with ν being the kinematic viscosity of the fluid, and ρ the density of the fluid.

2.1.2 Efimtsov model [28]

The single-point wall-pressure spectrum Φ_p is calculated as:

$$\Phi(\omega) = \frac{2\pi\alpha u_t^3 \rho^2 \delta\beta}{(1 + 8\alpha^2 \left(\frac{\omega\delta}{u_\tau}\right)^2)^{1/3} + \alpha\beta Re_\tau((\frac{\omega\delta}{u_\tau})/Re_\tau)^{10/3}} \quad (3)$$

$$\beta = [\,1 + \left(\frac{Re_{\tau 0}}{Re_\tau}\right)^3\,]^{1/3} \quad (4)$$

$$T_\omega = T + \left(1 + 0.89\frac{\gamma - 1}{2}M^2\right) \quad (5)$$

where, Re_τ is the shear stress Reynolds number given by $Re_\tau = \frac{\delta u_\tau}{\upsilon_\omega}$; absolute viscosity of fluid $\upsilon_\omega = \upsilon\frac{\rho}{\rho_\omega}(\frac{T_\omega}{T})^{0.89}$ and density of fluid is given by $\rho_\omega = \rho\frac{T}{T_\omega}$

2.1.3 Rackl-Weston model [6]

Two semi-empirical corrective functions were added to the Efimtsov Model [28] to better anticipate a broadband peak around a Strouhal number of 0.6 and to regulate the high-frequency roll-off of the PSD.

$$\phi(f) = \phi(f)_{Efimtsov} + x_1(f) + x_2(f) \quad (6)$$

where the corrective functions are,

$$x_1(f) = \frac{1}{4}\left[\tanh(\log_{10}\left(\frac{f}{1000}\right)\right) + 1]\,[M - 1.65]\log_{10}(f) \quad (7)$$

$$x_2(f) = 2.5\, e^{(-\left(\ln\left(\frac{2\pi\delta^*}{U_\infty}\right)(f)\right) - \ln(0.6))^2)} \quad (8)$$

All other spectrum models are detailed in their respective articles. In-house MATLAB codes are used to estimate wall-pressure spectrum for each model, compared with wind tunnel experiment and in-flight test data, and presented in the later section.

2.2 Simulation of Turbulent Flow over Flat Plate using RANS Models

The problem statement is explained with the help of the schematic diagram in Figure 1. This is as per the experimental setup of Salze *et al.,* [8] which has been further described by Lenevue *et al.,* [14]. A flat plate with dimensions $650 \times 300 \times 1\text{mm}$ is placed in the wind tunnel. The walls are subjected to zero pressure gradient. A rectangular domain of length 2050 mm and 250 mm height is considered for numerical simulation, where the flat plate is placed 1400 mm from the flow inlet. Two points are chosen at x = 1495 mm. (Point-1, pink) and x = 1595 mm. (Point-2, blue) as per the experimental setup. In the present work, gravity has not been considered and the fluid is incompressible.

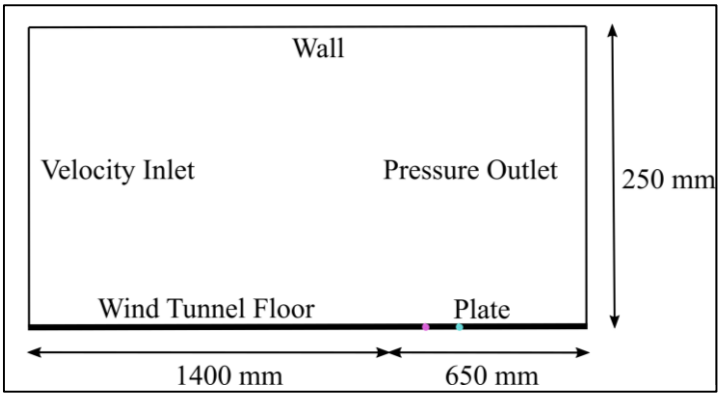

Fig. 1. Schematic of the domain for flat plate TBL simulation

The basic equations on turbulent flow are explained in detail by Adanta *et al.,* [33]. The flow variables on simulating the turbulent boundary layer over the flat plate is calculated by the incompressible Reynolds Averaged Navier Stokes (RANS) equations and the Reynolds stresses are modelled using the linear eddy-viscosity model following Boussinesq hypothesis [18]. The closure of the RANS equations has been achieved by the model proposed by Wilcox [20], namely the $k - \omega$ model. The study has been thoroughly compared using the other closure models, like that of the $k - \varepsilon$ model, proposed by Launder and Sharma [19]; the $k - \omega$ shear stress transport (SST) model proposed by Menter [21, 22] with updated empirical model constants and blending functions; the one-equation Spalart Allmaras model proposed by Spalart and Allmaras [23] and the realizable $k - \varepsilon$ model proposed by Shih [24]. For these turbulence closure models, the original damping functions and model constants have been adopted.

The RANS equation in tensor notation can be written as:

$$\frac{\partial(\rho U_i)}{\partial t} + \frac{\partial(\rho U_i U_j)}{\partial x_j} = -\frac{\partial P}{\partial x_i} + \frac{\partial}{\partial x_j}\left[\mu\left(\frac{\partial U_i}{\partial x_j} + \frac{\partial U_j}{\partial x_i}\right) - \rho\overline{u_i' u_j'}\right] \tag{9}$$

where, 'U' is the mean flow velocity (m/s) in i^{th} or j^{th} directions (2D), 'P' is the pressure, 't' is time (s), ρ is the fluid density (kg/m^3), μ is the absolute viscosity of the fluid (Pa-s).

The Reynolds stresses are solved using the Boussinesq constitutive relation [18] or Eddy-viscosity model,

$$-\rho\overline{u'v'} = \mu_t \frac{\partial U}{\partial y} \tag{10}$$

μ_t is a fictitious quantity for which the modeling is shifted from Reynolds stress tensor to eddy viscosity (μ_t), thus the naming. Further, it controls the strength of diffusion, that is, more the μ_t, more is the transfer of momentum from faster to slower-moving fluid particles.

As the order of multiplication does not matter, so the shear stress components can be written as such:

$$-\rho\overline{u'v'} = -\rho\overline{v'u'} = \mu_t \left(\frac{\partial U}{\partial y} + \frac{\partial V}{\partial x}\right) \tag{11}$$

This is why the Reynolds stress tensor is symmetric and there are six independent components. Eq. (10) and Eq. (11) are the diagonal terms of the Reynolds stress tensor, but for the normal components, Eq. (11) becomes,

$$-\rho\overline{u'v'} = 2\mu_t \frac{\partial U}{\partial y} \quad (12)$$

Now, by the definition of turbulent kinetic energy (k), it is the sum of the Reynolds stress terms. But, by adding the Reynolds stress terms, an inconsistent solution of turbulent kinetic energy is obtained, as shown below:

$$-\rho\ (\underline{\acute{u}\acute{u}} + \underline{\acute{v}\acute{v}} + \underline{\acute{w}\acute{w}}) = 2\mu_t\ (\frac{\partial U}{\partial y} + \frac{\partial V}{\partial x} + \frac{\partial W}{\partial z}) \quad (13)$$

As, $k = \frac{1}{2}\ (\underline{\acute{u}\acute{u}} + \underline{\acute{v}\acute{v}} + \underline{\acute{w}\acute{w}})$

So, sum of the normal components of Reynolds stress terms should be

$$-\rho\ (\underline{\acute{u}\acute{u}} + \underline{\acute{v}\acute{v}} + \underline{\acute{w}\acute{w}}) = 2\rho k \quad (14)$$

which is not equal to Eq. (13).

Again, for an incompressible flow, Eq. (12) and Eq. (13) become inconsistent,because

$$\frac{\partial U}{\partial y} + \frac{\partial V}{\partial x} + \frac{\partial W}{\partial z} = 0 \quad (15)$$

Therefore 1/3rd of the sum of the normal components is subtracted from the over predicting error Reynolds stress term giving

$$-\rho\underline{\acute{u}\acute{u}} = 2\mu_t\ \{\frac{\partial U}{\partial x} - \frac{1}{3}(\frac{\partial U}{\partial x} + \frac{\partial V}{\partial y} + \frac{\partial W}{\partial z})\} - \frac{1}{3}(2\rho k) \quad (16)$$

$$-\rho\underline{\acute{v}\acute{v}} = 2\mu_t\ \{\frac{\partial V}{\partial y} - \frac{1}{3}(\frac{\partial U}{\partial x} + \frac{\partial V}{\partial y} + \frac{\partial W}{\partial z})\} - \frac{1}{3}(2\rho k) \quad (17)$$

$$-\rho\underline{\acute{w}\acute{w}} = 2\mu_t\ \{\frac{\partial W}{\partial z} - \frac{1}{3}(\frac{\partial U}{\partial x} + \frac{\partial V}{\partial y} + \frac{\partial W}{\partial z})\} - \frac{1}{3}(2\rho k) \quad (18)$$

This is done, so that the summation of these equations, that is, the normal components justify the turbulent kinetic energy.

Writing Eq. (11), Eq. (16), Eq. (17) and Eq. (18) combined in tensor notation, in terms of mean rate of strain tensor (S_{ij}) and it's deviatoric part ($S_{ij}{}^*$)

$$-\rho\overline{u_i'u_j'} = 2\mu_t(\ S_{ij} - \frac{1}{3}\frac{\partial U_k}{\partial x_k}\delta_{ij}) - \frac{2}{3}\rho k\delta_{ij} \quad (19)$$

$$-\rho\overline{u_i'u_j'} = 2\mu_t S_{ij}{}^* - \frac{2}{3}\rho k\delta_{ij} \quad (20)$$

Shear stresses can be written as
Mean rate of strain tensor:

$$S_{ij} = \mu_t(\frac{\partial U_i}{\partial x_j} + \frac{\partial U_j}{\partial x_i}) \quad (21)$$

where, the repeated indices (k, k) represent summation and δ_{ij} is the Kronecker delta,

δ_{ij}= {1 $for\ i = j\ and\ 0\ for\ i \neq j$

In OpenFOAM, Eq. (20) is depicted as:

$$- \rho\overline{u'u'} = \mu_t[\nabla U+(\nabla U)^T]-\frac{1}{3}(\nabla U)I\ -\frac{2}{3}\rho kI \quad (22)$$

where, δ_{ij}= {1 $for\ \ i = j\ and\ 0\ \ for\ \ i \neq j$ = $\begin{bmatrix}1 & 0 & 0\\ 0 & 1 & 0\\ 0 & 0 & 1\end{bmatrix}$

Depending on the turbulence model, the eddy-viscosity is calculated. To close the NS equations, various turbulence closure models have been developed over time by various researchers. Detailed derivation and review of governing equations in CFD is given by Yen *et al.,* [34]. The mathematical description of the different turbulence closure models, mentioned earlier is detailed next.

2.2.1 k-ε model [19]:

The eddy viscosity (μ_t) is related to turbulent kinetic energy (k) and turbulent dissipation rate (ε) as:

$$\mu_t = \rho C_\mu \frac{k^2}{\varepsilon}; \qquad C_\mu = 0.09 \quad (23)$$

The damping functions (f_1, f_2, f_μ), model coefficients (C_1, C_2, C_μ) that damp the dissipation rate close to the wall, and transport equations are detailed by Launder and Sharma [19].

Re_T = Turbulent Reynolds number = $\frac{\rho k^2}{\mu\epsilon}$; so $Re_T \sim \left(\frac{\rho UL}{\mu}\right)$ (24)

In low Re formulation, the eddy/turbulent viscosity is computed from k and epsilon as:

$$\mu_t = f_\mu C_\mu \frac{\rho k^2}{\epsilon} \quad (25)$$

The k – ε model initially was proposed to be applied when the first cell from the wall is present in the viscous sub-layer ($y^+ < 5$), like that in case of knowing wall shear stress and heat transfer applications. This is known as low-Re formulation. But over the years it has been found that k - ε model cannot accurately predict boundary layers with adverse pressure gradients like that required in aerodynamics and turbomachinery, for instance separation in the trailing edge of an aerofoil for high angle of attack and in diffusing sections where the area increases. If k - ε model is used then the point of separation of flow is predicted incorrectly and thus there are huge differences in the predicted flow parameters like coefficient of lift and drag than the actual ones.

The $k - \varepsilon$ model is thus used in high Re applications with $y^+ > 30$, for which the high Re formulations are required to be solved and there are no requirements of damping functions. To overcome the above-mentioned problem, various other turbulence models were developed with time.

2.2.2 k-ω model

ω is another representation of dissipation of turbulence, so often known as a specific turbulence dissipation rate, given by:

$$\omega = \frac{\epsilon}{C_\mu k}; \qquad C_\mu = 0.09 \tag{26}$$

This model is detailed in the work by Wilcox [20]**.** The transport equation for calculating ω,

$$\frac{\partial(\rho\omega)}{\partial t} + \nabla.(\rho\omega U) = \nabla.((\mu + \frac{\mu_t}{\sigma_k})\nabla\omega) + \frac{\gamma}{\nu_t} P_k - \beta\rho\omega^2 \tag{27}$$

The main difference between the above mentioned two turbulence models is that in k - ω model there are various empirical coefficients depending on the form of model being used. Choice of these coefficients in different solvers may alter the end results.

2.2.2.1 Limitations of k-ω model:

The k-ω model depends on the freestream turbulence conditions and small changes in freestream turbulent kinetic energy led to large changes in the turbulent viscosity and skin friction coefficient, as explained by Kok in Ref. [25]. This affects the forces on the body and flow separation inception. Now, for an adverse pressure gradient, the point of flow separation occurs where the coefficient of skin friction is zero and this depends on the freestream turbulence conditions. This is further explained in many literatures where it is said that the absence of cross diffusion term is the reason and Kok [25] suggested various values of the coefficients.

The remedy for this limitation of both the models was proposed by Menter [26]. A blend of both the models is used by using the k-epsilon model far away from the wall in the free stream when it is not susceptible to small changes in k and omega; and then near the wall the k-omega model is used. In between these, a blend of both the models is used which forms the basis of the k-omega SST (1992) model.

2.2.3 k-ω Shear Stress Transport (SST) model:

Menter [21] noticed that the k-ω BST model was overpredicting the wall shear stress, so the BST model was extended into the SST model with a viscosity limiter:

$$\text{Original: } \mu_t = \frac{\rho k}{\omega}; \qquad \text{SST Model: } \mu_t = \frac{a_1\,\rho k}{max\,(a_1\omega, SF_2)} \tag{28}$$

The purpose is to limit the viscosity thus reduce the wall shear stress to a more accurate level, closer to the experimental measurements of separated flow. 'S' is the magnitude of shear strain. F_2 is another blending function, which if large then viscosity is reduced.

$$F_2 = tanh\,(arg_2^2) \tag{29}$$

$$arg_2 = max\,(\frac{2\sqrt{k}}{\beta^*\omega d}, \frac{500\nu}{\omega d^2}) \tag{30}$$

'd' is the same as that for F_1 but can never be the wall normal distance 'y'. Further explanation is given by Menter [22].

It had been concluded that k - ω SST model is in better agreement to experiments for mildly separated flows, that is, external aerodynamics or simulations where separation is required.

2.2.4 Spalart Allmaras model

This model was proposed by Spalart and Allmaras [23] as an improvement over the k - ε model, to build a model that can simulate boundary layer for adverse pressure gradients. As stated by Kalitzin *et al.,* [27], the profile of ν_t near the wall of a flat plate, in the log-law region (y^+ > 30) is linear and in the viscous sub-layer (y^+ < 5), the profile is quartic, i.e., varies with $(y^+)^4$.

To resolve the quartic variation, the mesh needs to be quite fine close to the wall, as flow quantities vary linearly through cells in CFD. So, to solve this incongruity, instead of ν_t, a similar variable, the Spalart-Allmaras variable called $\tilde{\nu}$ is solved in order to make the solution more stable and easier with a smaller number of cells closer to the wall. $\tilde{\nu}$ varies linearly between ν_t and y^+. This linear profile is most suitable for flow over flat plates.

For boundary layer over a flat plate with zero pressure gradient,

$$\tilde{\nu} = \kappa y^+ \tag{31}$$

The linear profile near to a wall for finite Re is explained by Spalart and Allmaras [23]. The transport equation for the Spalart-Allmaras variable, $\tilde{\nu}$, is given by,

$$\frac{\partial \tilde{\nu}}{\partial t} + \nabla.(U\tilde{\nu}) = c_{b1}\bar{S}\,\tilde{\nu} + \frac{1}{\sigma}[\nabla.((\nu + \tilde{\nu})\nabla\tilde{\nu} + c_{b2}(\nabla\tilde{\nu})^2] - c_{w1}f_w(\frac{\tilde{\nu}}{d})^2 \tag{32}$$

which makes numerical solutions easier and tends to be linear on solving. $\tilde{\nu}$ is identical to ν_t, far away from the wall. $c_{b1}\bar{S}\,\tilde{\nu}$ = This term is for turbulence generation in the model. $\frac{1}{\sigma}[\nabla.((\nu + \tilde{\nu})\nabla\tilde{\nu} + c_{b2}(\nabla\tilde{\nu})^2$ = The diffusion term here has an additional non-linear term. This term is often split into a linear diffusion term, for the finite volume discretization and a non-linear explicit source term.

The term that shows the damping of turbulence near to any wall is, $c_{w1}f_w(\frac{\tilde{\nu}}{d})^2$ This is done by a combination of inviscid damping of pressure fluctuations and the viscous damping very close to the wall. The negative sign indicates destruction of turbulence. 'd' is the distance to the nearest wall and lesser 'd' indicates more turbulence destruction. $f_w \rightarrow 0$ as $d \rightarrow 0$ to prevent division by zero error.

The boundary conditions for $\tilde{\nu}$ is taken as $\tilde{\nu}$ = 0 at the wall for its linear behaviour in the viscous sub-layer. In the freestream, that is, far away from the wall, $\tilde{\nu}$ is taken to be the same as ν_t. So, at the inlet to the domain,

$$\tilde{\nu} = \nu_t = \frac{C_\mu k^2}{\epsilon} \text{ or } \tilde{\nu} = \nu_t = \frac{k}{\omega} \tag{33}$$

k and ω can be calculated from turbulent length scale, typically 10% of the aerofoil chord length and turbulence intensity, I, typically of 5%,

$$k = \frac{3}{2}U_\infty^2 I^2 \qquad \epsilon = C_\mu \frac{k^{3/2}}{l} \tag{34}$$

2.2.5 Realizable k–ε model

A new model dissipation rate equation based on the dynamic equation for fluctuating vorticity and a new realizable eddy viscosity formulation and a new eddy viscosity formulation had been proposed by Shih *et al.,* [24]. These equations ascertain realizability and hold the effect of mean rotation on turbulence stresses. Applications are in rotating homogeneous shear flows, channel and flat boundary layer flows with and without pressure gradients, boundary-free shear flows and backward facing step flows. This model is studied to be numerically more stable in turbulent flow calculations as the spreading rate anomaly of planar and round jets was removed completely.

3. Methodology

In this section mainly the mesh sensitivity studies are performed and quantified in terms of various convergence indices, along with discussion on the different the semi-empirical wall-pressure spectrum models and turbulence models. First, wind tunnel experiment and in-flight test are data are with experimental TBL parameters. Out of them, Smol'yakov – Tkachenko model [16] is found to be the best predictor of the wind tunnel test results as shown in Figure 4(a) and for in-flight test results, the Rackl-Weston model [6] is found to be the best predictor as shown in Figure 4(b).

Subsequently, a flat plate TBL wind tunnel experiment conducted by Salze *et al.,* [8] is numerically replicated. The schematic of the test case is shown in Figure 1 and simulation is performed using five RANS turbulence closure models, namely:

i. Standard k – ω
ii. k – ω SST
iii. k – ε
iv. Realizable k – ε
v. Spalart-Allmaras

Mesh sensitivity studies for the flat plate boundary layer case done by Salze *et al.,* [8] are first performed separately using OpenFOAM and ANSYS Fluent solvers for different RANS models. Next, these two solvers are employed to simulate the flow field and extract the TBL parameters in alignment with the experiment at two different locations (point 1: 1495mm and point 2: 1595mm downstream of the domain inlet) and at two different wind speeds (30 m/s and 50 m/s). Then, different CFD models with different y+ values are compared with experimental results both at the component level (U_τ, δ, δ^*, θ) and pressure spectrum level (Φ_p). Finally, sensitivity mapping is performed between a particular spectrum model and a particular CFD setup and presented.

Three types of meshing with uniform rectangular cells in 2D plane are studied for both OpenFOAM and Fluent solvers and are presented in Table 1. A section of the mesh for the mesh sensitivity study has been shown from Figure 2(a) to Figure 2(c). The representative cell length (h) is calculated as, $h = \frac{1}{N}\sum_{cell} A_p^{1/2}$, where N is the number of cells and A_p, is the area of each cell.

Table 1
Three different 2D meshes

Mesh	Number of cells	Representative Cell Length (h) [m]
Coarse	60000	0.0029
Medium	120000	0.0021
Fine	240000	0.0015

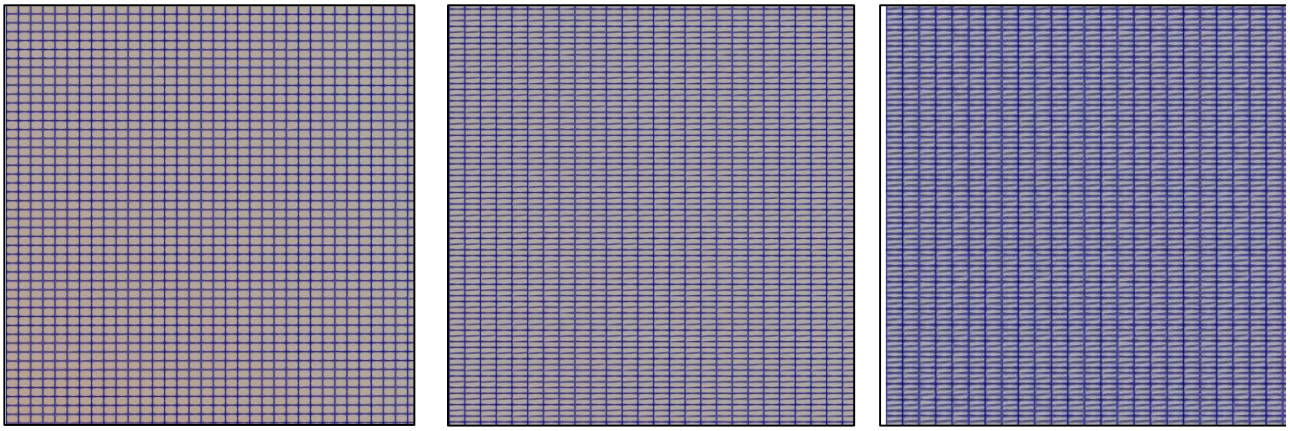

(a) (b) (c)

Fig. 2. Mesh (a) Coarse (b) Medium (c) Fine

The present meshing satisfies the recommendations of Celik *et al.,* [17], that the representative cell lengths should be at least 30% different for each mesh. The most ideal mesh is having an infinite number of cells, corresponding to a representative cell length (RCL) (h) approaching zero, estimated using Richardson extrapolation technique. On designating fine, medium, and coarse mesh as 1, 2, and 3, respectively, friction velocity at h = 0 can be expressed as,

$$U_{\tau 0} = \frac{r_{21}^{p} U_{\tau 1} - U_{\tau 2}}{r_{21}^{p} - 1} \tag{35}$$

where refinement ratio, $r_{21} = \frac{h_2}{h_1}$, and p is the order of convergence. The order of convergence p is estimated using the method proposed by Celik *et al.,* [11] as it is a more general approach suitable for both monotonic and oscillatory convergence. In the beginning, differences in calculated friction velocities are determined for the fine mesh-medium mesh (ϵ_{21}), and the medium mesh-coarse mesh (ϵ_{32}) as:

$$\epsilon_{21} = U_{\tau 2} - U_{\tau 1}; \epsilon_{32} = U_{\tau 3} - U_{\tau 2} \tag{36}$$

Next, their ratio is calculated to find $s = sign(\frac{\epsilon_{32}}{\epsilon_{21}})$. The final form of the implicit non-linear equation is:

$$\frac{1}{ln(r_{21})} \left| ln \left| \frac{\epsilon_{32}}{\epsilon_{31}} \right| + ln \left(\frac{r_{21}^{p} - s}{r_{32}^{p} - s} \right) \right| - p = 0 \tag{37}$$

This equation is solved using the Newton-Raphson iteration technique. In the present mesh sensitivity study, *three* types of errors are estimated for each case, namely relative error (e_{21}), extrapolated relative error (e_{21}^{ext}), and Grid Convergence Index (GCI_{21}).

$$e_{21} = \left| \frac{U_{\tau 2} - U_{\tau 1}}{U_{\tau 1}} \right|; \; e_{21}^{ext} = \left| \frac{U_{\tau 1} - U_{\tau 0}}{U_{\tau 0}} \right|; \; GCI_{21} = \left| \frac{e_{21}}{r_{21}^{p} - 1} \right| \tag{38}$$

The formulation for normalized wall distance, y^{+}, describing various grid convergence is provided belo, along with the estimation of δ^{*} and θ from the CFD-obtained velocity profiles. For all the studied cases these parameters are calculated using in-house MATLAB scripts.

$$y^+ = \frac{y_p U_\tau}{\nu} \tag{39}$$

where y_p is the distance of the centroid of the first cell adjacent to the wall. Displacement thickness (δ^*) and momentum thickness

$$\delta^* = \sum_{i=2}^{N-1}(1 - \frac{u_i}{U_0})\left(\frac{y_{i+1}-y_{i-1}}{2}\right) \tag{40}$$

$$\theta = \sum_{i=2}^{N-1}\frac{u_i}{U_0}(1 - \frac{u_i}{U_0})\left(\frac{y_{i+1}-y_{i-1}}{2}\right) \tag{41}$$

The numerical set up for the present work is done in a way to simulate the experimental set up given by Salze *et al.,* [8]. The mesh for clustering and convergence, for varying y^+ and for flow velocity 30 m/s has been presented in Figure 3(a) to Figure 3(c). The mesh for y^+ = 1 and y^+ = 30 has been given for an elevation of the entire fluid domain over the flat plate. The mesh for y^+ = 100 is having a BF of 1, so only a magnified section has been presented here. The entire BF results are shown in Table 6 and Table 7.

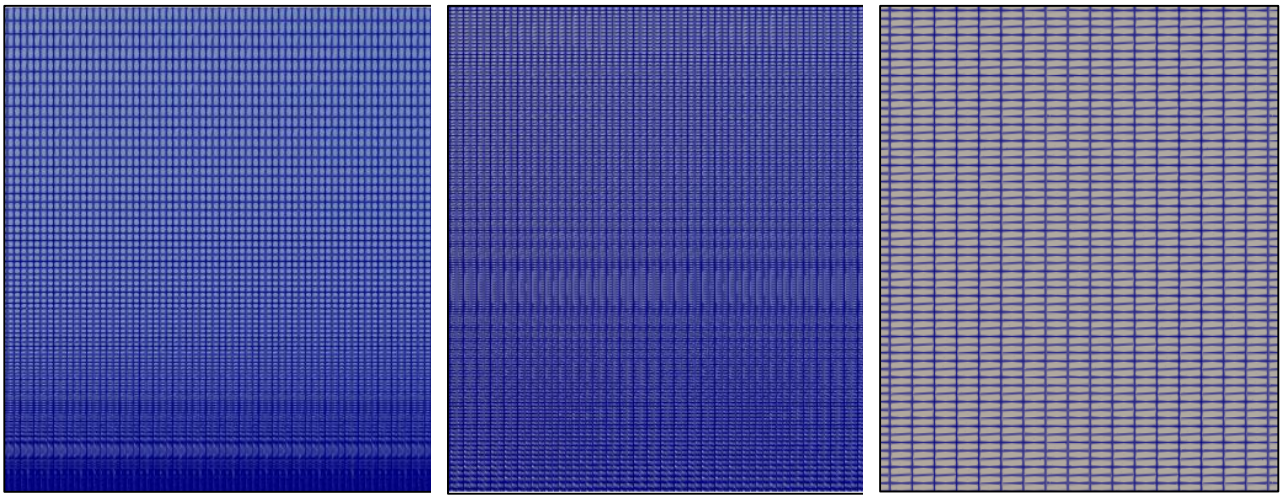

(a) (b) (c)

Fig. 3. Mesh for $y^+$for U = 30 m/s (a) y^+ = 1 (b) y^+ = 30 (c) y^+ = 100

4. Results

4.1 Comparison of Spectrum Models with Wind Tunnel PSD

Several semi-empirical spectrum models are compared with PSD values from wind tunnel experiment conducted by Goody and Simpson [5] and Rackl-Weston's in-flight test [6], and presented in Figure 4(a) and Figure 4(b). The experimental spectrum is single-sided, for a two-dimensional ZPG flow as described by Thomson and Rocha [11]. They used naturally developed turbulent boundary layers to study wall-pressure fluctuations.

The findings are in-line with Thomson and Rocha [11] as Goody [12] and Smol'yakov [13] spectrum models are found to be the best in terms of replicating the wind tunnel test. The study presented ascertains this finding, but in addition shows that Smol'yakov and Tkachenko model [16] is also a good predictor of the wind tunnel test results along with Goody [12], Smol'yakov [13] and Lagnelli [32] models as can be seen in Figure 4(a). The present study is performed on Smol'yakov and

Tkachenko model [16] as for practical purpose it is found to be providing better estimation of TBL-induced plate vibration in the low-frequency regime [35].

Similar study has been done with various semi-empirical models by comparing them with the PSD values from in-flight test data conducted by Rackl and Weston [6], presented in Figure 4(b) and Rackl and Weston spectrum model [6] certainly is found to be predicting the best.

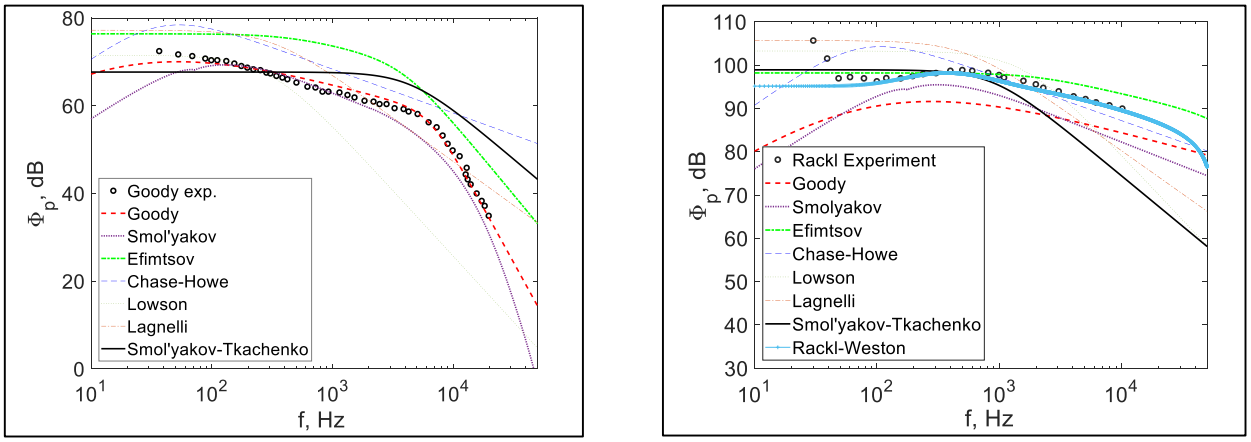

(a) (b)

Fig. 4. Comparison of wall-spectrum models with (a) Goody-Simpson wind tunnel experiment [5] (b) Rackl and Weston in-flight test data [6] Ref. $4 \times 10^{-10}\ Pa^2$

4.2 CFD: Mesh Sensitivity Study

The sensitivity of friction velocity to various mesh sizes is studied using the equations Eq. (35) to Eq. (38) at two different locations, for all the five turbulence models, with free stream velocity (U_∞) 30 m/s and 50 m/s using OpenFOAM [36] and Fluent. Out of these 40 combinations, only *four* results are presented in Table 2 to Table 5 as representative results. The mesh sensitivity study is performed by referencing the friction velocity value obtained from the experiment conducted by Salze *et al.,* [8] and presented in Figure 5(a) - 5(d). 'h' is the representative cell length (RCL).

Table 2
Point 1; $k-\omega$ SST; OpenFOAM; $U_\infty = 30m/s$

RCL (h) [m]	U_τ [m/s]	$U_\tau\ extr$ [m/s]	e_{21} [%]	e_{21}^{ext} [%]	GCI_{21}
0.0015	1.156	1.159	0.19	0.29	0.36
0.0021	1.154				
0.0029	1.159				

Table 3
Point 1; $k-\omega$ SST; Fluent; $U_\infty = 30m/s$

RCL (h) [m]	U_τ [m/s]	$U_\tau\ extr$ [m/s]	e_{21} [%]	e_{21}^{ext} [%]	GCI_{21}
0.0015	1.140	1.140	0.00	0.00	0.00
0.0021	1.140				
0.0029	1.150				

Table 4
Point 2; $k-\omega$ SST; OpenFOAM; $U_\infty = 30m/s$

RCL (h) [m]	U_τ [m/s]	U_τ *extr* [m/s]	e_{21} [%]	e_{21}^{ext} [%]	GCI_{21}
0.0015	1.151	1.156	0.22	0.48	0.60
0.0021	1.148				
0.0029	1.153				

Table 5
Point 2; $k-\omega$ SST; Fluent; $U_\infty = 30m/s$

RCL (h) [m]	U_τ [m/s]	U_τ *extr* [m/s]	e_{21} [%]	e_{21}^{ext} [%]	GCI_{21}
0.0015	1.130	1.120	0.88	0.93	1.15
0.0021	1.140				
0.0029	1.150				

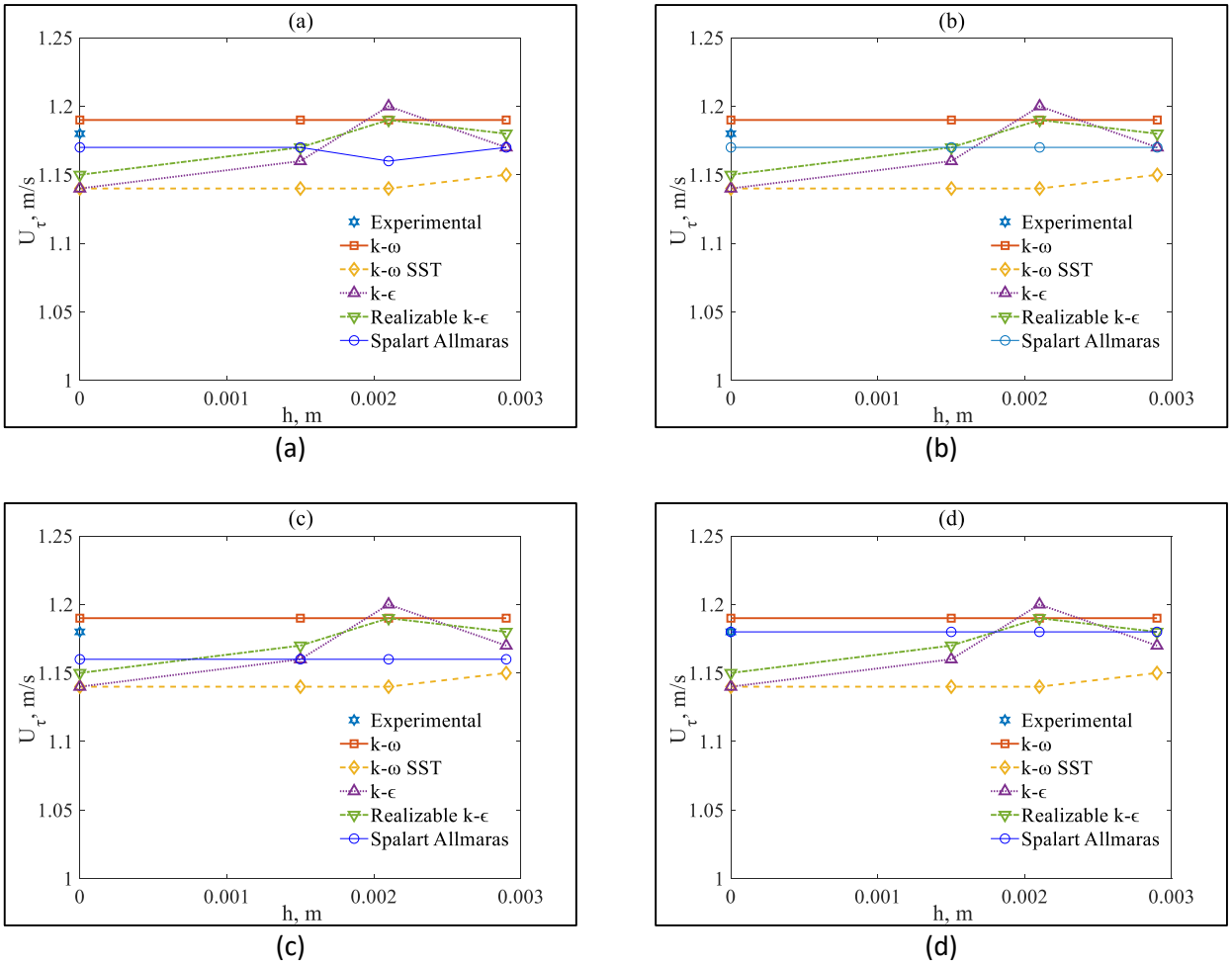

Fig. 5. (a) Point 1; $U_\infty = 30m/s$; OpenFOAM (b) Point 1; $U_\infty = 30m/s$; ANSYS Fluent (c) Point 2; $U_\infty = 30m/s$; OpenFOAM (d) Point 2; $U_\infty = 30m/s$; ANSYS Fluent

As observed from the mesh sensitivity studies, it is found that the 'medium' mesh is sufficient for all subsequent studies, and thus the accuracy analysis of different CFD variants is conducted with this meshing. Different solvers (OpenFOAM, Fluent), turbulence models ($k-\omega$, $k-\omega$ SST, $k-\epsilon$ and Realizable $k-\epsilon$, Spalart Allmaras), and y^+ values (1, 30, and 100) are examined with the experimental values ($U_\tau, \delta, \delta^*, \theta$) as obtained by Salze *et al.,* [8].

4.2.1 CFD simulation; part 1: clustering and convergence

To simulate TBL parameters properly, near-wall grid clustering is performed using the Eq. (39) to Eq. (41). For different y^+ values, the first cell height ($2y_p$) is initially calculated as per Eq. (39) and is presented in Table 6 and Table 7 for flow velocity 30 m/s and 50 m/s respectively. Bias Factor (BF) is the ratio of last cell height to the first cell height. Figure 6 and Figure 7 depict universal velocity plots.

Table 6
y^+ calculation for U = 30m/s

y^+	U [m/s]	v [10^{-5} m^2/s]	$2y_p$ [10^{-5} m]	Biasing Factor
1	1.18	1.46	2.47	284.3
30			74.5	2.6
100			247	1

Table 7
y^+ calculation for U = 50m/s

y^+	U [m/s]	v [10^{-5} m^2/s]	$2y_p$ [10^{-5} m]	Biasing Factor
1	1.18	1.46	1.55	496.29
30			46.5	5.64
100			155	1

Typical convergence is shown in Figure 6 and Figure 7 for the realizable $k-\epsilon$ model at two different locations with $U_\infty = 30\ m/s$, where $U^+ = \frac{U}{U_\tau}$, U is the local velocity and U_τ is the friction velocity.

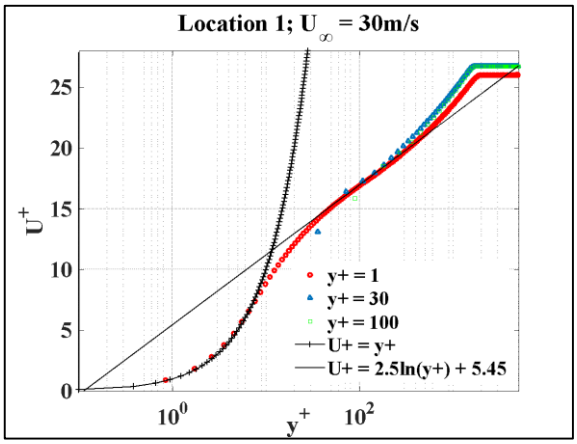

Fig. 6. Universal velocity plot; OpenFOAM

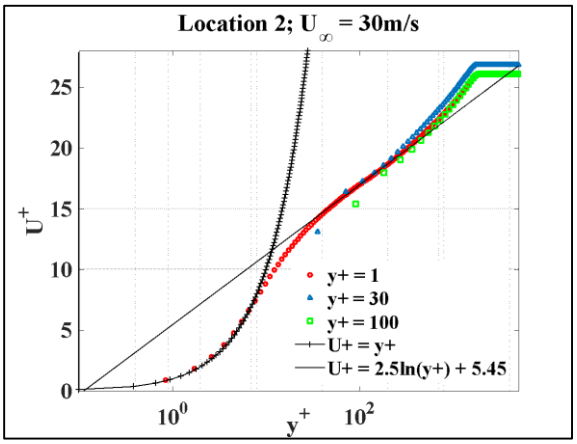

Fig. 7. Universal velocity plot; OpenFOAM

The detailed results of sensitivity of mean square pressure for wind tunnel experiment on all the RANS turbulence models mentioned is given in Table 8 and Table 9. Table 8 details the error of the mean square pressure as obtained from experimentally and numerically at Point 1. Similarly, Table 9 details the error of the mean square pressure as obtained from experimentally and numerically at Point 2.

Table 8
Experimental and numerical parameters; Point 1; $U_\infty = 30$ m/s

Model	Solver	y^+	U_τ	δ	δ^*	θ	$\bar{p}^2$(ST)	$\bar{p}^2$ (RW)
Experimental values			1.18	29.54	4.04	3.14	28.955	29.59
SA	OpenFOAM	1	1.15	24.5	3	2.1	25.6123	23.34
		30	1.17	24.8	3.3	2.2	27.7158	25.9
		100	1.16	26.5	3.4	2.2	27.11	25.83
	Fluent	1	1.22	29.83	2.9	2.2	33.2	34.58
		30	1.17	30.99	3.4	2.1	27.54	29.21
		100	1.17	30	3.8	2	27.63	28.71
$k-\omega$	OpenFOAM	1	1.14	21.3	3	2.1	25.2628	24.66
		30	1.19	23.8	3.4	2.3	29.8032	30.54
		100	1.183	25.75	3.5	2.3	29.1847	29.45
	Fluent	1	1.19	28.14	3	2.2	30.1158	29.95
		30	1.19	29.21	3.5	2.2	29.7268	30.56
		100	1.19	28.75	4	2.1	29.7522	30.3
$k-\omega$ SST	OpenFOAM	1	1.12	22.3	3	2.1	23.6346	20.03
		30	1.16	23	3.3	2.2	26.7371	23.9
		100	1.154	21.75	3.3	2.1	26.4095	22.62
	Fluent	1	1.17	21.6	3.1	2.2	27.504	23.99
		30	1.14	23.99	3.5	2.1	25.0066	22.6
		100	1.14	22.5	4.1	2.1	25.4995	21.81
$k-\epsilon$	OpenFOAM	1	1.53	33.5	5.2	3.6	81.6805	101.6
		30	1.19	23.8	3.3	2.2	30.2481	27.35
		100	1.183	22.8	3.3	2.1	29.1794	26
	Fluent	1	1.12	22.3	3	2.1	23.6346	20.03
		30	1.16	23	3.3	2.2	26.7371	23.9
		100	1.154	21.75	3.3	2.1	26.4095	22.62
R $k-\epsilon$	OpenFOAM	1	1.4	30.8	3.9	2.3	57.3563	64.32
		30	1.1	28.75	3.3	2.2	21.7601	21.22
		100	1.14	40	3.4	2.1	25.1857	29.67
	Fluent	1	1.39	29.83	4.4	3.1	55.4239	62.26
		30	1.14	23.99	3.5	2.1	24.9943	22.6
		100	1.14	25	3.9	2.1	25.4154	23.12

ST = Smol'yakov and Tkachenko, RW = Rackl and Weston

Table 9
Experimental and numerical parameters; Point 1; $U_\infty = 50\ \mathrm{m/s}$

Model	Solver	y^+	U_τ	δ	δ^*	θ	$\bar{p}^2$(ST)	$\bar{p}^2$ (RW)
Experimental values			**1.89**	23	**3.37**	**2.58**	188.8705	263.33
SA	OpenFOAM	1	1.87	23	2.8	2	180.0016	204.76
		30	1.86	23.8	3	2	176.5348	203.56
		100	1.86	25.25	3.2	2	175.4397	209.91
	Fluent	1	1.95	30.5	2.7	2.1	214.35	284.76
		30	1.87	29.7	3	2	180.91	233.53
		100	1.87	31.3	3.6	1.9	180.62	239.75
$k-\omega$	OpenFOAM	1	1.83	21.3	2.8	2	163.8959	222.69
		30	1.89	22.8	3.1	2.1	189.0555	261.77
		100	1.89	23	3.3	2.1	187.4897	259.41
	Fluent	1	1.95	27.73	2.7	2.1	214.3511	271.43
		30	1.9	30.4	3	2	193.0304	253.5
		100	1.9	30	3.7	2	193.662	251.82
$k-\omega$ SST	OpenFOAM	1	1.79	24.8	2.7	1.9	152.0452	175.38
		30	2.08	34.5	2.4	1.7	276.8019	401.82
		100	1.84	25	3	1.9	169.9854	199.05
	Fluent	1	1.87	20.82	2.8	2.1	179.0819	194.24
		30	1.82	20.9	3	2	162.8651	172.55
		100	1.84	21.3	3.8	2	168.5817	182.98
$k-\epsilon$	OpenFOAM	1	2.42	31.5	4.7	3.3	511.9758	740.91
		30	1.89	22.3	3	2	188.9635	211.19
		100	1.884	21.5	3.1	2	186.0652	204.24
	Fluent	1	2.36	32.49	4.4	3.1	463.3937	675.29
		30	1.87	24.82	3	2	179.6693	213.13
		100	1.86	25	3.7	2	178.6657	208.83
R $k-\epsilon$	OpenFOAM	1	2.31	32.75	3.5	2.9	421.818	618.19
		30	1.79	28	3.1	2.1	153.2422	193
		100	1.83	36.25	3.1	1.9	165.6821	234.27
	Fluent	1	2.21	27.73	4	2.8	352.8618	469.76
		30	1.82	20.85	3	2	162.7226	172.32
		100	1.84	22.5	3.7	1.9	168.165	188.38

ST = Smol'yakov and Tkachenko, RW = Rackl and Weston

4.2.2 CFD simulation; part 2: component error analysis

The accuracy of the turbulence models with various y^+ is analyzed in terms of estimating TBL components, and the error % are presented in the form of stacked bar graphs in Figure 8(a) to Figure 8(d). The stacks on each bar represent the amount of error with respect to the wind tunnel experiment results as obtained by Salze *et al.,* [8]. The mean square pressure (MSP) is obtained by fetching the flow variables in the Smol'yakov-Tkachenko Model [16]. The accuracy of the best predicting model, $k-\omega$ model, is presented here. It can be observed that in spite of the considerable error amounts of the flow parameters obtained between experiment and CFD, the final error amount in mean square pressure is quite less.

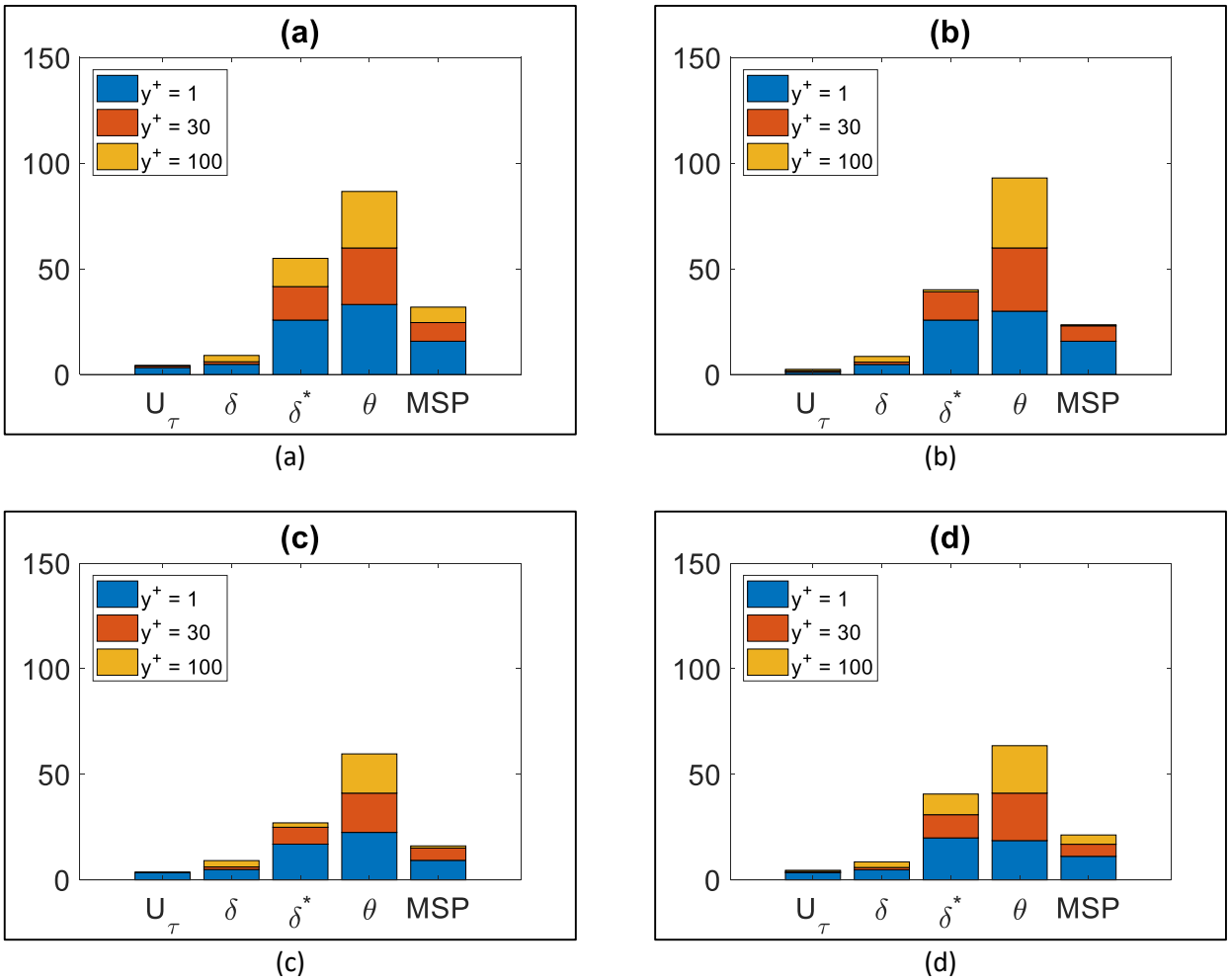

Fig. 8. (a) Point 1; U_∞ = 30m/s; OpenFOAM, $k-\omega$ model [20], Smol'yakov-Tkachenko Model [16] (b) Point 1; U_∞ = 30m/s; ANSYS Fluent, $k-\omega$ model [20], Smol'yakov-Tkachenko Model [16] (c) Point 1; U_∞ = 50m/s; OpenFOAM, $k-\omega$ model [20], Smol'yakov-Tkachenko Model [16] (d) Point 1; U_∞ = 50m/s; ANSYS Fluent, $k-\omega$ model [20], Smol'yakov-Tkachenko Model [16]

Similarly, the accuracy of the turbulence models with various y^+ is analysed by comparing with Rackl-Weston Model [6], in terms of estimating TBL components, and presented in the stacked bar graphs in Figure 9(a) to Figure 9(d). The accuracy of the best predicting model, $k-\omega$ model, is presented here. Similar observation has been obtained here as well.

The detailed results on the experimental values and the numerical estimation of shear velocity (U_τ), boundary layer thickness (δ), boundary layer displacement thickness (δ^*), momentum

thickness (θ), mean square pressure fluctuations ($\bar{p}^2$) for Point-1, $U_\infty = 30$ m/s, are detailed in Table-8 (Refer to Appendix) and that of for Point-1, $U_\infty = 50$ m/s, are detailed in Table-9 (Refer to Appendix).

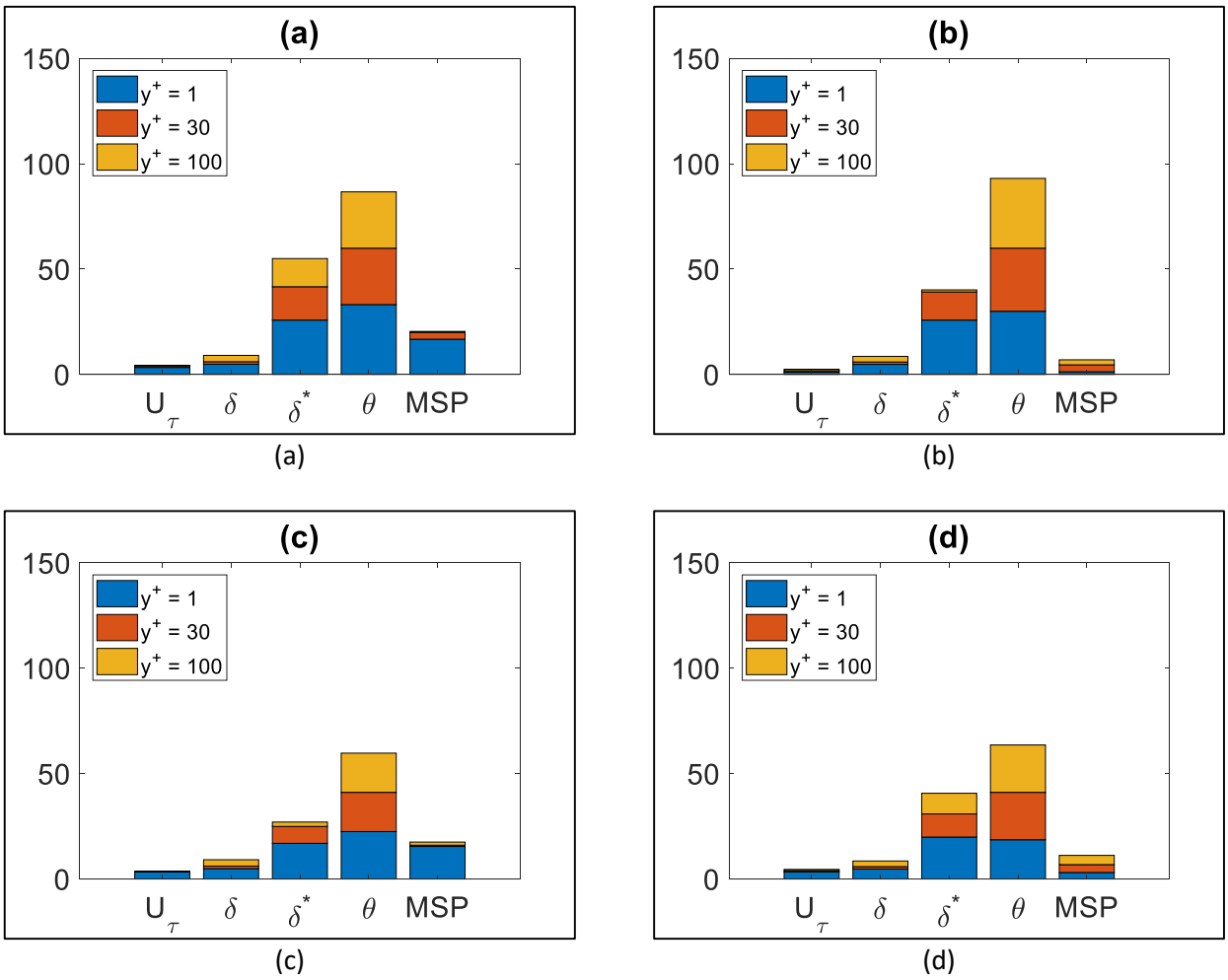

Fig. 9. (a) Point 1; U_∞ = 30m/s; OpenFOAM, $k-\omega$ model [20], Rackl-Weston Model [6] (b) Point 1; U_∞ = 30m/s; ANSYS Fluent, $k-\omega$ model [20], Rackl-Weston Model [6] (c) Point 1; U_∞ = 50m/s; OpenFOAM, $k-\omega$ model [20], Rackl-Weston Model [6] (d) Point 2; U_∞ = 50m/s; ANSYS Fluent, $k-\omega$ model [20], Rackl-Weston Model [6]

4.2.3 CFD simulation; part 3: $\bar{p}^2$ error analysis

Initially, the single-sided wall pressure spectra (Φ_p) are calculated using Goody [12], Smol'yakov [13] and Smol'yakov-Tkachenko [16] models for the CFD-obtained TBL parameters. As the best prediction is done by putting the TBL parameters obtained from CFD in the Smol'yakov Tkachenko Model, so the results corresponding to that model are presented here. Subsequently, the summation of the spectrum over its collapsing frequency (50 kHz for the present case) is done as per Eq. (42) and the mean square of pressure fluctuations ($\bar{p}^2$) are estimated.

$$\bar{p}^2 = \int_0^\infty \Phi_p(f)\, df \tag{42}$$

Finally, a comparison is done with the experimental ($\bar{p}^2$) values. This is a practical approach as it accounts for the global energy over the entire frequency range and not the local pressure PSD values.

A grid independence study is performed and results are presented in Figure 10 to Figure 13 in the form of $\bar{p}^2$ vs. y^+. The Richardson extrapolation technique as discussed in Eq. (35) through Eq. (38) for friction velocity is used same as it is for $\bar{p}^2$ to obtain the MSP value for the finest possible grid clustering ($y^+ = 0$), $\bar{p}^2{}_0$. This extensive study:

i. Shows the convergence of different turbulence models as the y^+ tends to ZERO.
ii. Error in MSP calculation for different CFD configurations, w.r.t. the experimental values.
iii. Clearly distinguish the contribution of turbulence models, spectrum models, y^+, location and flow velocity towards the final error.

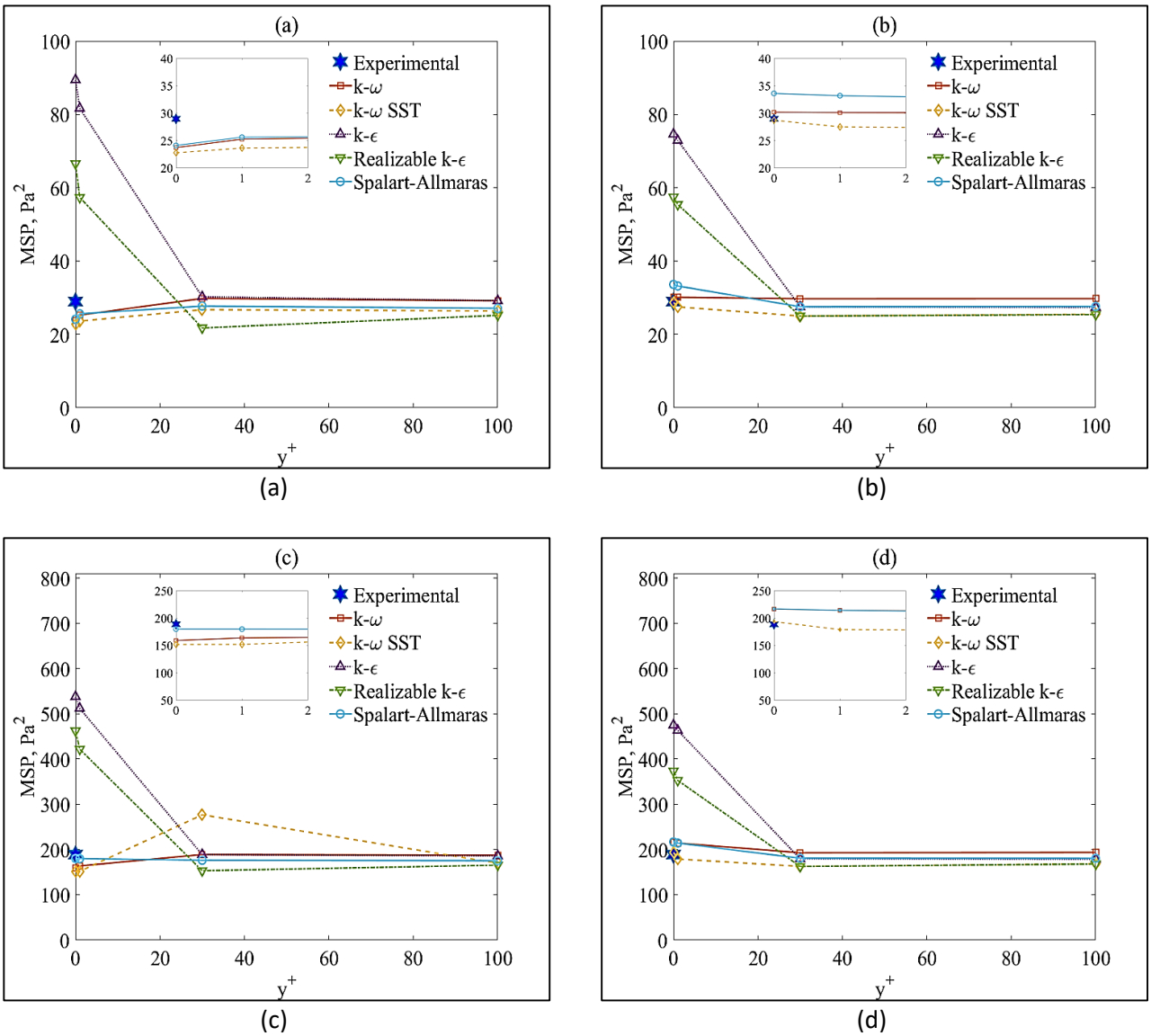

Fig. 10. (a) Convergence of $\bar{p}^2$ (MSP) with y^+. Point 1; U_∞ = 30m/s; OpenFOAM, Smol'yakov-Tkachenko Model [16] (b) Convergence of $\bar{p}^2$ (MSP) with y^+. Point 1; U_∞ = 30m/s; ANSYS Fluent, Smol'yakov-Tkachenko Model [16] (c) Convergence of $\bar{p}^2$ (MSP) with y^+. Point 1; U_∞ = 50m/s; OpenFOAM, Smol'yakov-Tkachenko Model [16] (d) Convergence of $\bar{p}^2$ (MSP) with y^+. Point 1; U_∞ = 50m/s; ANSYS Fluent, Smol'yakov-Tkachenko Model [16]

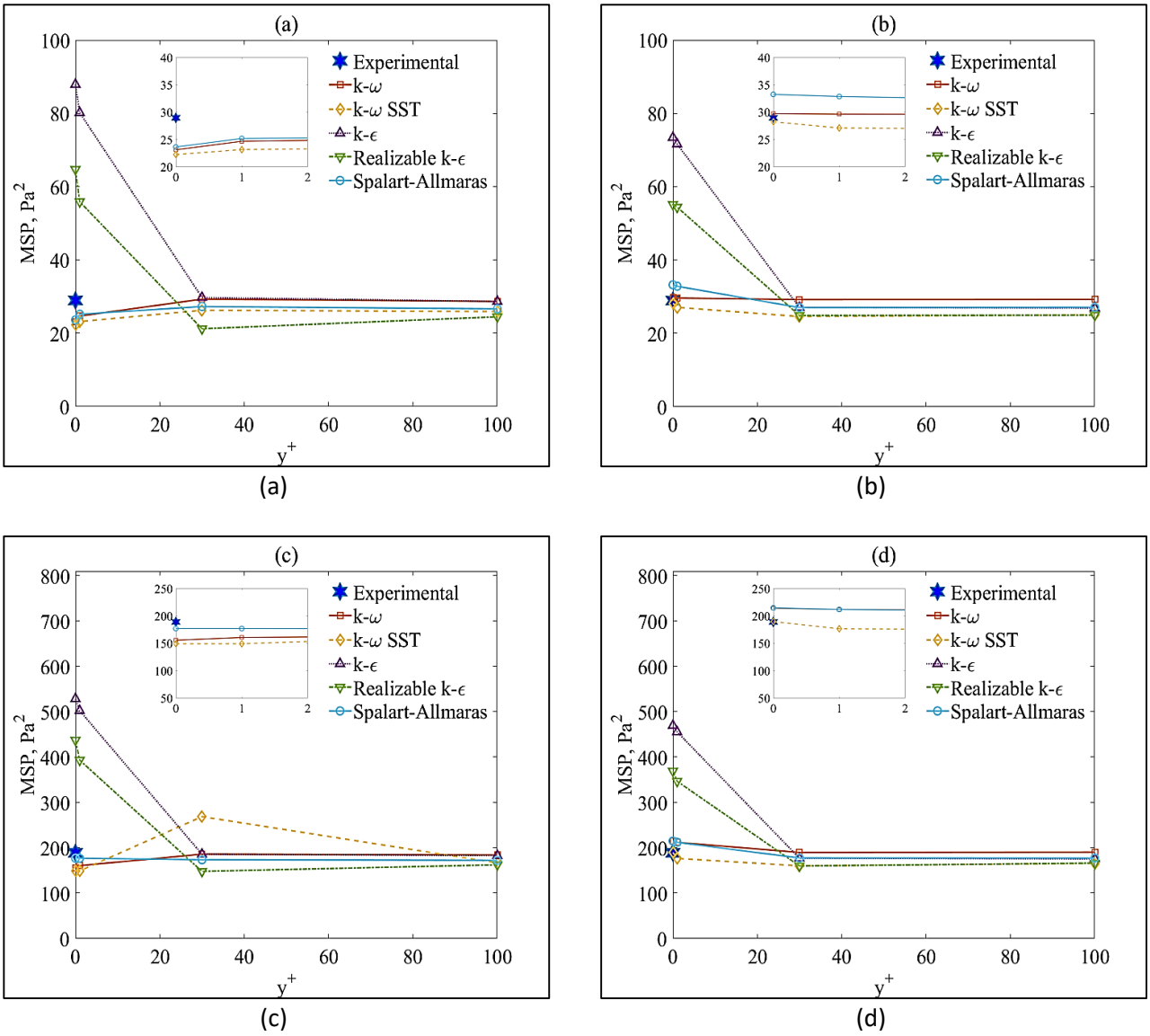

Fig. 11. (a) Convergence of $\bar{p}^2$ (MSP) with y^+. Point 2; U_∞ = 30m/s; OpenFOAM, Smol'yakov-Tkachenko Model [16] (b) Convergence of $\bar{p}^2$ (MSP) with y^+. Point 2; U_∞ = 30m/s; ANSYS Fluent, $k-\omega$ model [20], Smol'yakov-Tkachenko Model [16] (c) Convergence of $\bar{p}^2$ (MSP) with y^+. Point 2; U_∞ = 50m/s; OpenFOAM, Smol'yakov-Tkachenko Model [16] (d) Convergence of $\bar{p}^2$ (MSP) with y^+. Point 2; U_∞ = 50m/s; ANSYS Fluent, Smol'yakov-Tkachenko Model [16]

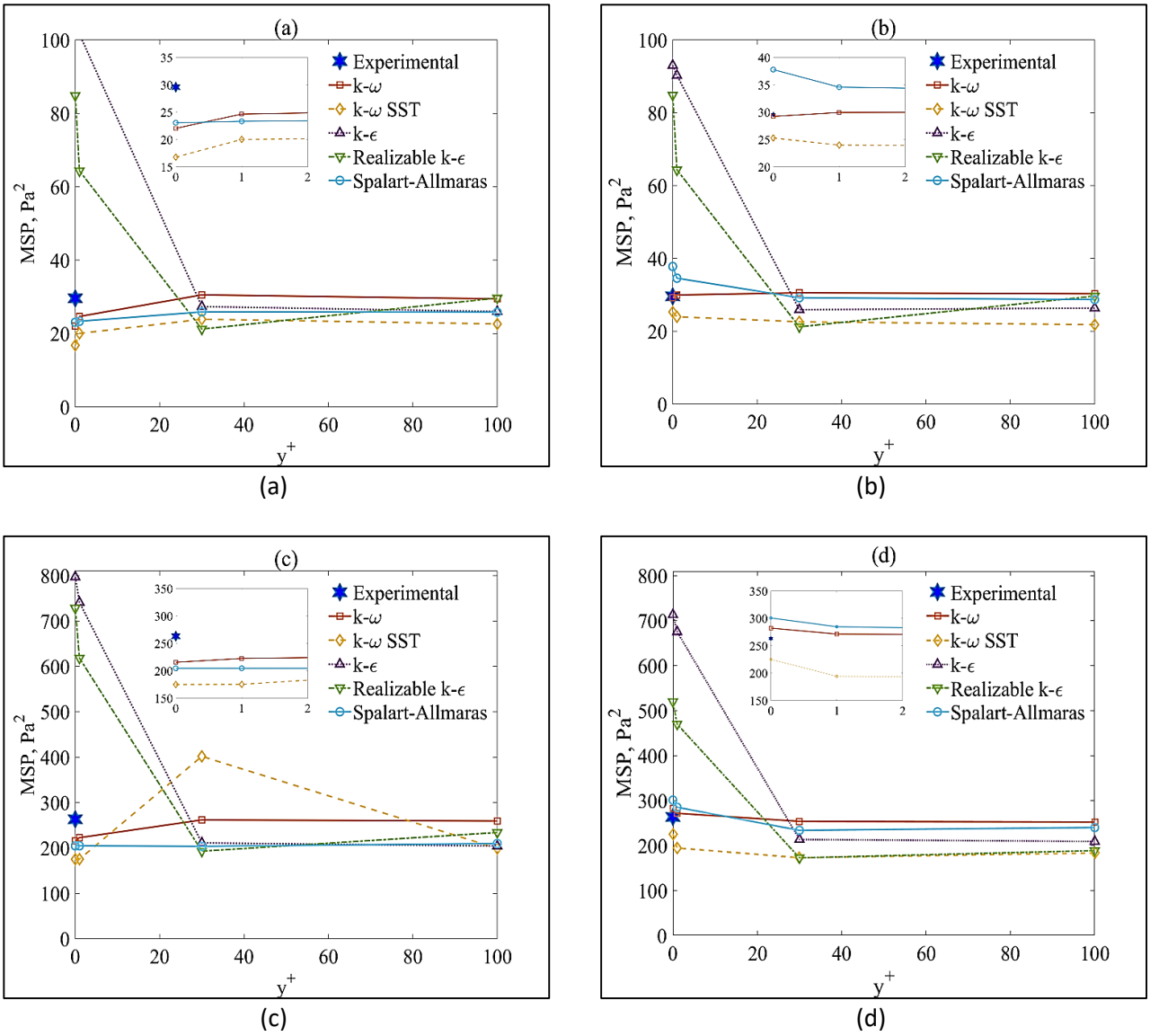

Fig. 12. (a) Convergence of $\bar{p}^2$ (MSP) with y^+. Point 1; U_∞ = 30m/s; OpenFOAM, Rackl-Weston Model [6] (b) Convergence of $\bar{p}^2$ (MSP) with y^+. Point 1; U_∞ = 30m/s; ANSYS Fluent, $k-\omega$ model [20], Rackl-Weston Model [6] (c) Convergence of $\bar{p}^2$ (MSP) with y^+. Point 1; U_∞ = 50m/s; OpenFOAM, Rackl-Weston Model [6] (d) Convergence of $\bar{p}^2$ (MSP) with y^+. Point 1; U_∞ = 50m/s; ANSYS Fluent, Rackl-Weston Model [6]

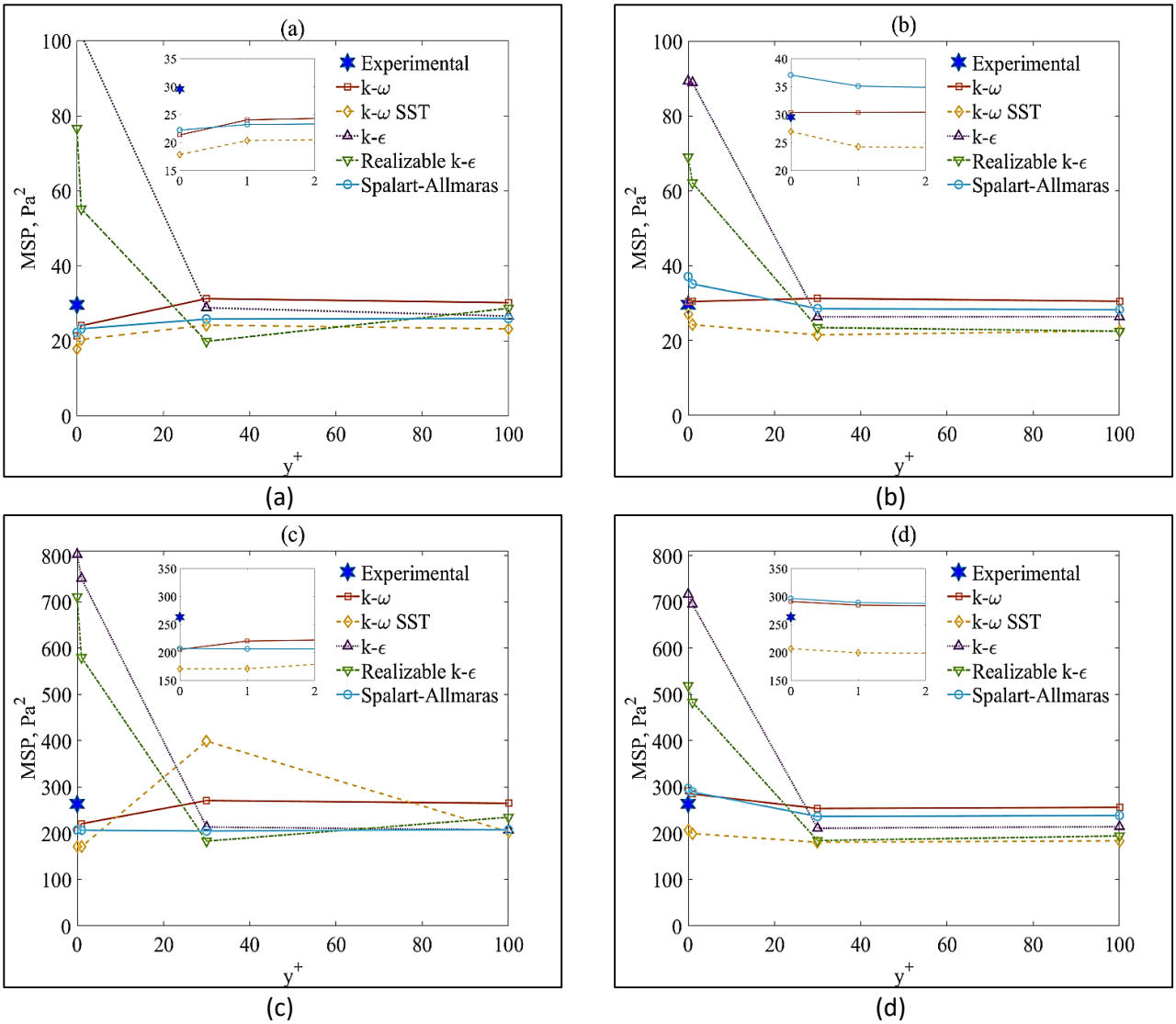

Fig. 13. (a) Convergence of $\bar{p}^2$ (MSP) with y^+. Point 2; U_∞ = 30m/s; OpenFOAM, Rackl-Weston Model [6] (b) Convergence of $\bar{p}^2$ (MSP) with y^+. Point 2; U_∞ = 30m/s; ANSYS Fluent, $k-\omega$ model [20], Rackl-Weston Model [6] (c) Convergence of $\bar{p}^2$ (MSP) with y^+. Point 2; U_∞ = 50m/s; OpenFOAM, Rackl-Weston Model [6] (d) Convergence of $\bar{p}^2$ (MSP) with y^+. Point 2; U_∞ = 50m/s; ANSYS Fluent, Rackl-Weston Model [6]

The grid convergence results of MSP show a clear pattern that the Spalart-Allmaras, $k-\omega$ and $k-\omega$ SST turbulence models are quite reliable in terms of convergence of the numerical schemes. Moreover, they calculate MSP values with a very good accuracy w.r.t the MSP values estimated with the experimental TBL wall parameters. This observation remains valid irrespective of the solver, location or the flow velocities within the study range. $k-\epsilon$ family of models ($k-\epsilon$ and realizable $k-\epsilon$) are found to be diverging whenever the y^+ value comes close to zero. It is expected as these models does not capture the near-wall flow well. Although, these models can suitably be used for $y^+ > 30$, if required. This marginal value can change if further study is carried out in the zone of $1 < y^+ < 30$.

Among the turbulence models $k-\omega$ is in general found to be the best predictor for Smol'yakov and Tkachenko model, and Rackl and Weston model. Overall, $k-\omega$ family of models along with Spalart-Allmaras one equation model in some cases are recommended for flat plate TBL pressure fluctuation estimation. $k-\epsilon$ family of models are not suggested for these type of near wall

investigations due to its numerical divergence and magnified error in the near wall region. This happens because the $k - \omega$ model is generally found to be better at resolving the eddies at y^+ less than 5, than the $k - \varepsilon$ or realizable $k - \varepsilon$ model. In practice, there is high dissipation [37] of turbulent kinetic energy near walls, shear layer and where turbulence is going to be high. Moreover, $k - \omega$ model is better performer for aerodynamics and turbomachinery which the k - ε model is not, as explained earlier. This is because in the $k - \varepsilon$ model the damping functions (f_1, f_2, f_μ) used are not that accurate in the presence of adverse pressure gradients. But $k - \omega$ family of models does not need these damping functions when adverse pressure gradient is present.

As, $k - \omega$ family of models is found to be the best predicting RANS turbulence models, so error analysis for $k - \omega$ model is presented in Table 10 for Point 1, ST model; Table 11 for Point 2, ST model; Table 12 for Point 1, RW model and Table 13 for point 2, RW model.

The typical error analysis of MSP estimation using different y^+ values are presented in Table 10 to Table 13.

Table 10
Error in $\bar{p}^2$ estimation (in %); point 1; Smol'yakov-Tkachenko model

Model	y^+	30 m/s		50 m/s	
		Open FOAM	Fluent	Open FOAM	Fluent
$k - \omega$	1	15.72	15.72	9.25	11.15
	30	8.84	7.31	5.83	5.72
	100	7.31	0.49	1.01	-4.40

Table 11
Error in $\bar{p}^2$ estimation (in %); point 2; Smol'yakov-Tkachenko model

Model	y^+	30 m/s		50 m/s	
		Open FOAM	Fluent	Open FOAM	Fluent
$k - \omega$	1	12.12	13.88	10.91	12.77
	30	5.83	5.83	4.27	7.44
	100	4.42	**-0.72**	**0.79**	**-2.57**

Table 12
Error in $\bar{p}^2$ estimation (in %); point 1; Rackl-Weston Model

Model	y^+	30 m/s		50 m/s	
		Open FOAM	Fluent	Open FOAM	Fluent
$k - \omega$	1	-16.68	1.23	-15.43	3.08
	30	3.22	3.27	-0.59	-3.73
	100	-0.48	2.40	-1.49	-4.37

Table 13
Error in $\bar{p}^2$ estimation (in %); point 2; Rackl-Weston Model

Model	y^+	30 m/s		50 m/s	
		Open FOAM	Fluent	Open FOAM	Fluent
$k - \omega$	1	-18.67	2.81	-16.20	8.14
	30	5.67	5.66	2.78	-3.66
	100	2.01	3.03	0.56	-2.77

5. Conclusion

The two-fold sensitivity of the zero-pressure gradient flat plate turbulent boundary layer wall-pressure spectrum is investigated for flow over flat plate. One aspect of this sensitivity lies in the approximations of the pressure spectrum models. Another important part deals with the variation in mean square pressure fluctuations caused by the choice of model parameters like solver, near wall grid clustering, measuring location and the flow velocity. The study is performed by numerically replicating the wind tunnel experiments and in-flight tests considering different RANS configurations. Smol'yakov-Tkachenko model for wind tunnel experiments, and Rackl-Weston model for in-flight tests are observed to be a fair point to start with. The $k - \omega$ family of models are found to be the best predictor of MSP with very good convergence, when experimental wall parameters are fed into the spectrum models, and compared. $k - \epsilon$ family of models are recommended to be avoided for this type of near wall studies.

Thus, the present study has been able to bridge the gap in selection of a suitable RANS turbulence closure model for predicting the wall pressure parameters with compatible grid clustering and suitable wall-pressure spectrum models. Also, it addresses the split in the error contribution; one part is the suitability of the pressure spectrum models, and another one is the choice of CFD model parameters.

Acknowledgement
This research is funded by Department of Science and Technology, Government of West Bengal, India.

References

[1] Schewe, Günter. "On the structure and resolution of wall-pressure fluctuations associated with turbulent boundary-layer flow." *Journal of Fluid Mechanics* 134 (1983): 311-328. https://doi.org/10.1017/S0022112083003389

[2] McGrath, Brian E., and Roger L. Simpson. *Some features of surface pressure fluctuations in turbulent boundary layers with zero and favorable pressure gradients*. No. NAS 1.26: 4051. NASA, 1987.

[3] Farabee, Theodore M., and Mario J. Casarella. "Spectral features of wall pressure fluctuations beneath turbulent boundary layers." *Physics of Fluids A: Fluid Dynamics* 3, no. 10 (1991): 2410-2420. https://doi.org/10.1063/1.858179

[4] Gravante, S. P., A. M. Naguib, C. E. Wark, and HMm Nagib. "Characterization of the pressure fluctuations under a fully developed turbulent boundary layer." *AIAA journal* 36, no. 10 (1998): 1808-1816. https://doi.org/10.2514/2.296

[5] Goody, Michael C., and Roger L. Simpson. "Surface pressure fluctuations beneath two-and three-dimensional turbulent boundary layers." *AIAA journal* 38, no. 10 (2000): 1822-1831. https://doi.org/10.2514/2.863

[6] Rackl, Robert, and Adam Weston. *Modeling of turbulent boundary layer surface pressure fluctuation auto and cross spectra-verification and adjustments based on TU-144LL data*. No. NASA/CR-2005-213938. 2005.

[7] Rocha, Joana, and Daniel Palumbo. "On the sensitivity of sound power radiated by aircraft panels to turbulent boundary layer parameters." *Journal of Sound and Vibration* 331, no. 21 (2012): 4785-4806. https://doi.org/10.1016/j.jsv.2012.05.030

[8] Salze, Édouard, Christophe Bailly, Olivier Marsden, Emmanuel Jondeau, and Daniel Juvé. "An experimental characterisation of wall pressure wavevector-frequency spectra in the presence of pressure gradients." In *20th AIAA/CEAS Aeroacoustics Conference*, p. 2909. 2014. https://doi.org/10.2514/6.2014-2909

[9] Blitterswyk, Van, and Jared Corey. "Experimental characterization of turbulent motions using wall-pressure measurements in low Reynolds number turbulent boundary layers." PhD diss., Carleton University, 2016.

[10] Shahmohamadi, Hamed, and Mohammad Mehdi Rashidi. "Experimental investigation and a novel analytical solution of turbulent boundary layer flow over a flat plate in a wind tunnel." *International Journal of Mechanical Sciences* 133 (2017): 121-128. https://doi.org/10.1016/j.ijmecsci.2017.08.043

[11] Thomson, Nicholas, and Joana Rocha. "Comparison of Semi-Empirical Single Point Wall Pressure Spectrum Models with Experimental Data." *Fluids* 6, no. 8 (2021): 270. https://doi.org/10.3390/fluids6080270

[12] Goody, Michael. "Empirical spectral model of surface pressure fluctuations." *AIAA journal* 42, no. 9 (2004): 1788-1794. https://doi.org/10.2514/1.9433
[13] Smol'yakov, A. V. "Calculation of the spectra of pseudosound wall-pressure fluctuations in turbulent boundary layers." *Acoustical Physics* 46, no. 3 (2000): 342-347. http://dx.doi.org/10.1134/1.29890
[14] Leneveu, Romain, Martin Rissman, and Alberto A. Pinar. "Validation with experimental data of an heterogeneous turbulent wall pressure fluctuation model in a FEM structural context." In *25th AIAA/CEAS Aeroacoustics Conference*, p. 2751. 2019. https://doi.org/10.2514/6.2019-2751
[15] Dominique, J., J. Van den Berghe, C. Schram, and M. A. Mendez. "Artificial neural networks modeling of wall pressure spectra beneath turbulent boundary layers." *Physics of Fluids* 34, no. 3 (2022): 035119. https://doi.org/10.1063/5.0083241
[16] Smol'Yakov, A. V., V. M. Tkachenko, and J. S. Wood. "Model of a field of pseudosonic turbulent wall pressures and experimental data." *Soviet physics. Acoustics* 37, no. 6 (1991): 627-631.
[17] Celik, Ishmail B., Urmila Ghia, Patrick J. Roache, and Christopher J. Freitas. "Procedure for estimation and reporting of uncertainty due to discretization in CFD applications." *Journal of fluids Engineering-Transactions of the ASME* 130, no. 7 (2008). https://doi.org/10.1115/1.2960953
[18] Pope, Stephen B., and Stephen B. Pope. *Turbulent flows*. Cambridge university press, 2000.
[19] Launder, Brian Edward, and Bahrat I. Sharma. "Application of the energy-dissipation model of turbulence to the calculation of flow near a spinning disc." *Letters in heat and mass transfer* 1, no. 2 (1974): 131-137. https://doi.org/10.1016/0094-4548(74)90150-7
[20] Wilcox, David C. "Reassessment of the scale-determining equation for advanced turbulence models." *AIAA journal* 26, no. 11 (1988): 1299-1310. https://doi.org/10.2514/3.10041
[21] Menter, Florian R. "Two-equation eddy-viscosity turbulence models for engineering applications." *AIAA journal* 32, no. 8 (1994): 1598-1605. https://doi.org/10.2514/3.12149
[22] Menter, Florian R., Martin Kuntz, and Robin Langtry. "Ten years of industrial experience with the SST turbulence model." *Turbulence, heat and mass transfer* 4, no. 1 (2003): 625-632.
[23] Spalart, Philippe, and Steven Allmaras. "A one-equation turbulence model for aerodynamic flows." In *30th aerospace sciences meeting and exhibit*, p. 439. 1992. https://doi.org/10.2514/6.1992-439
[24] Shih, T-H., William W. Liou, Aamir Shabbir, Zhigang Yang, and Jiang Zhu. *A new k-epsilon eddy viscosity model for high Reynolds number turbulent flows: Model development and validation*. No. CMOTT-94-6. 1994.
[25] Kok, Johan C. "Resolving the dependence on freestream values for the k-turbulence model." *AIAA journal* 38, no. 7 (2000): 1292-1295.
[26] Menter, Florian R. "Influence of freestream values on k-omega turbulence model predictions." *AIAA journal* 30, no. 6 (1992): 1657-1659. https://doi.org/10.2514/3.11115
[27] Kalitzin, Georgi, Gorazd Medic, Gianluca Iaccarino, and Paul Durbin. "Near-wall behavior of RANS turbulence models and implications for wall functions." *Journal of Computational Physics* 204, no. 1 (2005): 265-291. https://doi.org/10.1016/j.jcp.2004.10.018
[28] Efimtsov, B., N. Kozlov, S. Kravchenko, and A. Andersson. "Wall pressure-fluctuation spectra at small forward-facing steps." In *5th AIAA/CEAS Aeroacoustics Conference and Exhibit*, p. 1964. 1999. https://doi.org/10.2514/6.1999-1964
[29] Lowson, Martin V. *Prediction of boundary layer pressure fluctuations*. WYLE LABS INC HUNTSVILLE AL TESTING DIV, 1968. https://doi.org/10.21236/AD0832715
[30] Chase, David M. "Modeling the wavevector-frequency spectrum of turbulent boundary layer wall pressure." *Journal of sound and Vibration* 70, no. 1 (1980): 29-67. https://doi.org/10.1016/0022-460X(80)90553-2
[31] Howe, Michael S., and Michael S. Howe. *Acoustics of fluid-structure interactions*. Cambridge university press, 1998. https://doi.org/10.1017/CBO9780511662898
[32] Laganelli, A. L., and H. F. Wolfe. "Prediction of fluctuating pressure in attached and separated turbulent boundary-layer flow." *Journal of Aircraft* 30, no. 6 (1993): 962-970. https://doi.org/10.2514/3.46440
[33] Adanta, Dendy, Budiarso Budiarso, and Ahmad Indra Siswantara. "Assessment of turbulence modelling for numerical simulations into pico hydro turbine." *Journal of Advanced Research in Fluid Mechanics and Thermal Sciences* 46, no. 1 (2018): 21-31.
[34] Tey, Wah Yen, Yutaka Asako, Nor Azwadi Che Sidik, and Rui Zher Goh. "Governing equations in computational fluid dynamics: Derivations and a recent review." *Progress in Energy and Environment* 1 (2017): 1-19.
[35] Hambric, S. A., Y. F. Hwang, and W. K. Bonness. "Vibrations of plates with clamped and free edges excited by low-speed turbulent boundary layer flow." Journal of fluids and structures 19, no. 1 (2004): 93-110. https://doi.org/10.1016/j.jfluidstructs.2003.09.002
[36] Ishak, Izuan Amin, Nurshafinaz Maruai, Fadhilah Mohd Sakri, Rahmah Mahmudin, Nor Afzanizam Samiran, Syabillah Sulaiman, Shaiful Fadzil Zainal Abidin, and Nik Normunira Mat Hassan. "Numerical Analysis on the Crosswind

Influence Around a Generic Train Moving on Different Bridge Configurations." *Journal of Advanced Research in Fluid Mechanics and Thermal Sciences* 89, no. 2 (2022): 76-98. https://doi.org/10.37934/arfmts.89.2.7698

[37] Beleri, Joonabi, and Asha S. Kotnurkar. "Peristaltic Transport of Ellis Fluid under the Influence of Viscous Dissipation Through a Non-Uniform Channel by Multi-Step Differential Transformation Method." *Journal of Advanced Research in Numerical Heat Transfer* 9, no. 1 (2022): 1-18.